Optical spectroscopy and ultrafast pump-probe study of the structural phase transition in $1T'$-$TaTe_2$

T. C. Hu,[1] Q. Wu,[1] Z. X. Wang,[1] L. Y. Shi,[1] Q. M. Liu,[1] L. Yue,[1] S. J. Zhang,[1] R. S. Li,[1] X. Y. Zhou,[1] S. X. Xu,[1] D. Wu,[1,2] T. Dong,[1] and N. L. Wang[1,2,*]

[1]*International Center for Quantum Materials, School of Physics, Peking University, Beijing 100871, China*

[2]*Beijing Academy of Quantum Information Sciences, Beijing 100913, China*

(Received 30 October 2021; revised 24 January 2022; accepted 25 January 2022; published 7 February 2022)

$1T'$-$TaTe_2$ exhibits an intriguing first-order structural phase transition at around 170 K. Understanding the electronic structural properties is a crucial way to comprehend the origin of this structural phase transition. We performed a combined optical and ultrafast pump-probe study on the compound across the transition temperature. The phase transition leads to abrupt changes in both optical spectra and ultrafast electronic relaxation dynamics. The measurements revealed a sudden reconstruction of the band structure. We elaborate that the phase transition is of first order and cannot be attributed to a conventional density-wave type instability. Our work is illuminating for understanding the origin of the structural phase transition.

DOI: 10.1103/PhysRevB.105.075113

I. INTRODUCTION

Transition-metal dichalcogenides (TMDs) have attracted tremendous interests for their intriguing ground states, physical properties, and potential applications [1–3]. Those low-dimensional compounds of these systems often lead to charge density wave (CDW) instability [4–8], yet many of those CDW-bearing materials are superconducting [9]. The interplay between the two very different cooperative electronic phenomena is one of the pending issues in condensed-matter physics. The origin of CDW is most commonly traced to Fermi surface nesting. However, the driving force for the higher-dimensional CDW formation in compounds is rather complex so that many mechanisms are being constantly proposed [10–15]. Compounds such as the well-known Ta/NbX_2 (X = S, Se, Te) with a $1T$ and $2H$ sandwich structure provide fundamental insight into the behavior of correlated electron systems. Among the TaX_2 (X = S, Se, Te) polytypes, the telluride $TaTe_2$ exhibits two intriguing commensurate CDW states but has not yet been well studied by spectroscopic techniques. Compared with the octahedral polymorphs $1T$-TaS_2 and $1T$-$TaSe_2$, $1T'$-$TaTe_2$ presents a stronger electron-phonon interaction and larger lattice distortion. The ground state of $TaTe_2$ is metallic rather than Mott insulating. The trimerization of Ta atoms in a $1T$ structure leads to double zigzag chains and an overall monoclinic distortion of the crystal lattice. So $TaTe_2$ can be regarded as a distorted $TaTe_6$ octahedral $1T'$ structure with a 3×1 ribbon-chain cluster superstructure at room temperature. Undergoing a structural phase transition at around 170 K, $TaTe_2$ transforms into a 3×3 butterflylike cluster superstructure [16,17]. The transition leads to an anomaly in specific heat, magnetic susceptibility, and electrical resistivity (a distinct kink structure with hysteresis) [17–19]. To date, no different polytypes with $1T$ and $2H$ structures have been found for $TaTe_2$. The low-temperature (LT) phase could be fully suppressed and a new superconducting phase could emerge at $T_c^{\text{onset}} \sim 1.7$–$2.5$ K when tellurium (Te) is partially replaced by selenium (Se) [20,21]. Additionally, applying an external pressure could achieve a bulk superconductivity of $TaTe_2$ between 4 and 6 K in the pressure range of 21–50 GPa [22]. As for the isostructural CDW compound $1T'$-$NbTe_2$ with a 3×1 superstructure at 300 K [23], such a LT phase has not been observed but exhibits superconductivity at $T_c \sim 0.5$ K [24]. Another analog layered compound $IrTe_2$ with a $5d$ heavy transition metal element and a strong Te-Te interlayer interaction shows an anomalous structural phase transition and transport properties as well [25], whereas the absence of a gap opening in $IrTe_2$ demonstrated by both an optical study and angle-resolved photoemission spectroscopy (ARPES), chemical bonding states, and crystal field splitting theory, were considered as origins of the transition [26,27].

It is essential to know the origin across different CDW states in two-dimensional CDW systems because of their close connection to superconductivity. Up to now, few theoretical works suggested that the CDW instability in $TaTe_2$ was driven by Fermi surface nesting [28,29]. On the other hand, limited experiment works mainly focused on measurements of the transport and structure properties [18,19,30–35]. Transport measurements suggested a possible occurrence of Fermi surface reconstruction just below T_s [18,19]. However, recently Kar *et al.* pointed out that the Fermi surface topology hardly changes across T_s by their ARPES study on $TaTe_2$ [36]. Available experiment results are still controversial. Other spectroscopy technique detections are still lacking. It is well known that optical and ultrafast spectroscopies are sensitive probes for the bulk electronic properties of solids. Therefore, it is significant to uncover the nature of the structural phase transition by the above techniques.

In this work, we performed combined temperature-dependent optical spectroscopy and ultrafast pump-probe

*nlwang@pku.edu.cn

measurements on a single-crystal $1T'$-$TaTe_2$ sample. The optical reflectivity spectra suddenly change just below T_s over a broad energy range, yielding evidence for the reconstruction of the band structure and an explicit reduction of the plasma frequency or the spectral weight of conducting carriers in the LT phase. However, no characteristic feature of an energy gap opening related to CDW formation is observed. An ultrafast pump-probe measurement reveals a dramatic change in the electronic relaxation dynamics near T_s. With the temperature increasing across T_s, the amplitude of transient reflectivity is enhanced enormously and the decay time becomes much faster. Furthermore, a number of coherent phonons in the LT phase were extracted by reflectivity oscillations in the time domain. Nevertheless, no amplitude mode of CDW collective excitation could be identified. In combination with the above experiment results we elaborate that the structural phase transition is not of a density wave type and cannot be simply attributed to a conventional Fermi surface nesting driven instability. Our work is illuminating for understanding the transitions of the different CDW states.

II. RESULTS AND DISCUSSION

Single crystals of $1T'$-$TaTe_2$ were synthesized by the chemical vapor transport method with iodine as the transport agent. High-purity Ta powders (99.99%) and Te pellets (99.999%) in a stoichiometric ratio (1:2) with additional iodine (99.8%, 5 mg/cm^3) were loaded into a quartz tube. All processes were operated in a sealed glove box. Then the quartz tube was sealed under high vacuum and heated at 560–480 °C in a two-zone furnace [31]. After 10 days growth, shiny platelike single crystals [typical size of $4 \times 2.5 \times 0.02$ mm^3, inset of Fig. 1(a)] were obtained. The temperature-dependent resistivity was measured by a standard four-probe method with a cooling/warming rate of 2 K/min in the *ab* plane. The measurement was performed in a Quantum Design physical property measurement system (PPMS). Resistivity measurements, shown in Fig. 1(a), indicate metallic behavior with a small resistivity value of about 2.1×10^{-4} Ω cm at 300 K. Similar to many two-dimensional CDW systems, $1T'$-$TaTe_2$ remains a metallic state at the LT phase and the residual resistance ratio (RRR $= \rho_{300\,\mathrm{K}}/\rho_{2\,\mathrm{K}}$) is about 14. The resistivity curve shows a significant kink hysteresis at around 160 K which suggests a first-order phase transition. X-ray diffraction (XRD) experiment results at room temperature are shown in Fig. 1(b). The strong diffraction peaks of $TaTe_2$ crystals can be indexed as (00L) of the monoclinic phase of $TaTe_2$ (ICDD-PDF21-1201). It can be seen that the full width at half maximum (FWHM) of the (001) Bragg peak is only about 0.05° in the inset of Fig. 1(b), indicating the high quality of the $TaTe_2$ single crystal. Detailed chemical compositions investigated by energy dispersive spectroscopy (EDS) measurements show that the chemical atomic ratios are close to the standard stoichiometric ratio (Ta : Te ∼ 1 : 1.96). All these sample fundamental characterizations are in good agreement with reports in the literature [17,31,34].

The as-grown *ab*-plane (001) optical reflectance measurements were performed on a Bruker 80V Fourier transform infrared spectrometer in the frequency range from 100 to 30 000 cm^{-1}. An *in situ* gold and aluminum evaporation technique was used to obtain the reflectance $R(\omega)$. The main panel of Fig. 2(a) shows the reflectivity up to 12 000 cm^{-1} at five selected temperatures. The inset displays the experimental reflectance spectrum up to 30 000 cm^{-1} at 300 K. A good metallic response is observed in the $R(\omega)$ spectrum: At low frequency, $R(\omega)$ has high values and approaches the unit at the zero-frequency limit. Below 4000 cm^{-1}, frequency-dependent reflectivity decreases almost linearly in the high-temperature (HT) phase. This behavior is similar to high-temperature cuprate superconductors. $R(\omega)$ shows a minor change as the temperature decreases from 300 to 180 K. However, when the temperature decreases just below the structural phase transition temperature at 160 K, optical reflectivity $R(\omega)$ shows an abrupt change. With further decreasing temperature, the spectral change becomes very small. The very low-frequency $R(\omega)$ increases slightly and forms a small plateau in the LT phase, reflecting enhanced metallic dc conductivity and consistent with the above resistivity measurements. In the meantime, two weak suppressions in the midinfrared region near 800 and 2300 cm^{-1} could be seen.

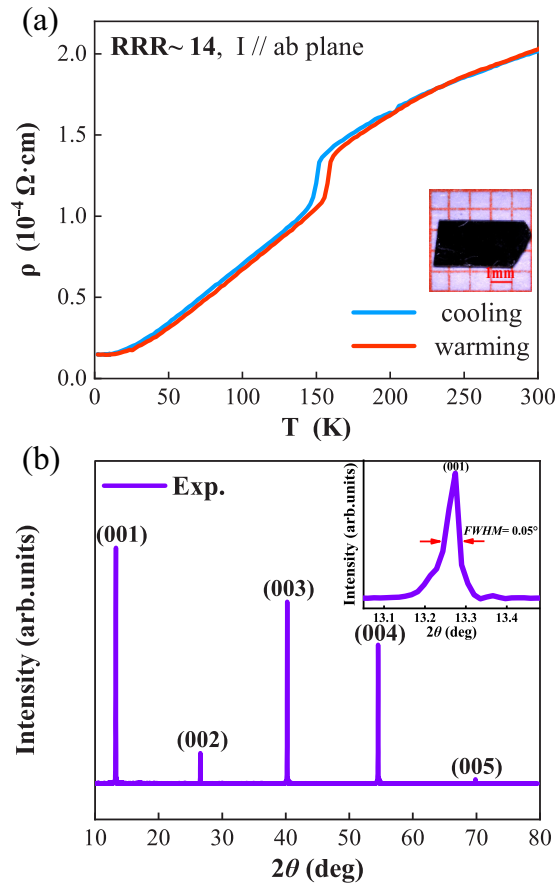

FIG. 1. Sample characterizations for $TaTe_2$. (a) Temperature-dependent *ab*-plane resistivity measurement. A structural phase transition is evident near 160 K. Inset: Single-crystal picture of $TaTe_2$. (b) Room-temperature powder XRD patterns of the single crystal and indexing. Inset: The full width at half maximum (FWHM) of the (001) Bragg peak is about 0.05°, indicating the good quality of the single crystal.

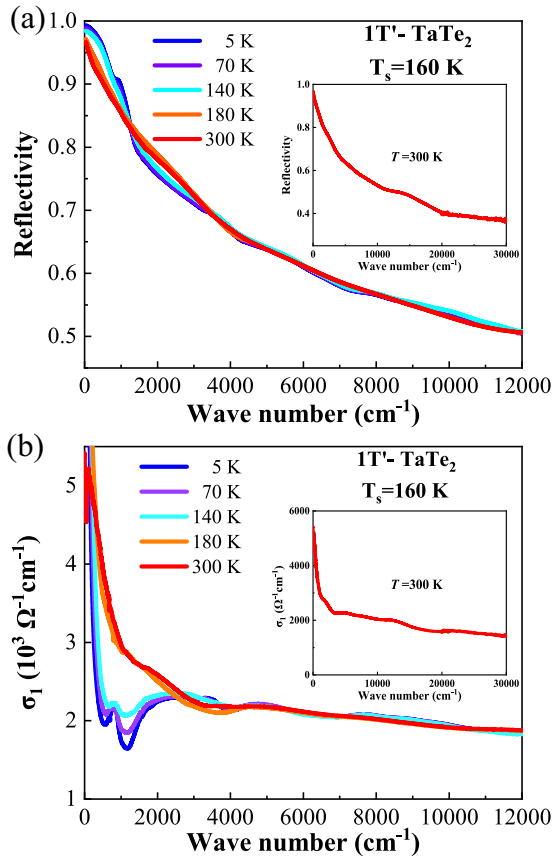

FIG. 2. Temperature-dependent optical spectroscopy of $TaTe_2$. (a) Temperature-dependent optical reflectivity measurements below 12 000 cm^{-1}. Inset: Large energy scale range of 100–30000 cm^{-1} at 300 K. (b) Temperature-dependent optical conductivity below 12 000 cm^{-1}. Inset: Optical conductivity spectrum with a large energy scale range of 100–30 000 cm^{-1} at 300 K.

The real part of optical conductivity $\sigma_1(\omega)$ was derived from $R(\omega)$ through a Kramers-Kronig transformation in Fig. 2(b). The Hagen-Rubens relation was used for the low-energy extrapolation of $R(\omega)$. We have employed x-ray atomic scattering functions in the high-energy side extrapolation [37]. The main panel of Fig. 2(b) displays $\sigma_1(\omega)$ below 12 000 cm^{-1} at five selected temperatures, and the inset displays $\sigma_1(\omega)$ up to 30 000 cm^{-1} at 300 K. Drude-type conductivity was observed in all spectra at a low frequency. In the HT phase, the broad width of the Drude peak indicates a large scattering rate of the itinerant carriers. Upon entering the LT phase, the weight of Drude-type conductivity was suddenly removed. The optical spectra were kept almost unchanged at 10 and 70 K. The overall spectral change reflects a significant band-structure reconstruction associated with the structural phase transition. In other words, there are two totally different metallic states in the HT and LT phases.

Actually, the formation of an energy gap with a relevant spectral change only at low energy is a key feature in the optical response for the CDW instability and associated structural phase transition. The so-called case-I factor of the CDW condensate would cause a sharp continuous rise in the optical conductivity spectra just above the energy gap. With the temperature further decreasing below the CDW phase transition the dip feature in reflectivity becomes more and more prominent. These features were observed clearly in most of the typical conventional CDW systems driven by Fermi surface nesting such as rare-earth tritelluride (RTe_3) [38], $LaAgSb_2$ [39], $Bi_2Rh_3Se_2$ [40], and CuTe [41]. On the contrary, for a purely structural phase transition being irrelevant to CDW order formation, the band structures of the HT and LT phases are entirely different. So the optical spectra would change suddenly over a broad range energy scale as observed in $BaNi_2As_2$ [42], $IrTe_2$ [26], and RuP [43]. For $TaTe_2$, the spectral change occurs in a wide frequency range and no continually evident reflectivity suppression is observed. The overall spectral change is similar to the latter characteristics which are attributed to the purely structural phase transition.

In order to isolate the different components of the electronic excitations and make a quantitative analysis, we employ the Drude-Lorentz model to decompose the optical conductivity. The Drude component represents the contribution from conduction electrons while the Lorentz components are used to describe the excitations across energy gaps and interband transitions. The general formula for the Drude-Lorentz model is

$$\sigma_1(\omega) = \sum_i \frac{\omega_{pi}^2}{4\pi} \frac{\Gamma_{Di}}{\omega^2 + \Gamma_{Di}^2} + \sum_j \frac{S_j^2}{4\pi} \frac{\Gamma_j \omega^2}{\left(\omega_j^2 - \omega^2\right)^2 + \omega^2 \Gamma_j^2}, \tag{1}$$

where ω_{pi} and Γ_{Di} are the plasma frequency and the relaxation rate of each conduction band while ω_j, Γ_j, and S_j represent resonance frequency, the damping, and the mode strength of each Lorentz oscillator, respectively. We found that two Drude components could roughly reproduce the low-frequency conductivity. This could be attributed to the multiband characteristic of $TaTe_2$ [20]. A similar two-Drude-component analysis has been applied to the optical data of $1T'$-$MoTe_2$ and T_d -WTe_2 [44], pointing towards a generic behavior for those multiband systems. The general formula for the Drude-Lorentz model is reproduced by two Drude components and one Lorentz oscillator at 300 K. Below the transition temperature, two additional Lorentz oscillators (Lorentz 2 and Lorentz 3) are required to fit the curve. Figures 3(a) and 3(b) show the spectra and fitting curves at two typical temperatures 300 and 5 K, respectively. The second Drude term is much broader and has a much larger spectral weight than the first one. In the LT phase at 5 K, both Drude terms shrink substantially and two more Lorentz (L2 and L3) oscillations centered at around 800 and 2300 cm^{-1} could be resolved.

The general plasma frequency is obtained as $\omega_p = (\omega_{p1}^2 + \omega_{p2}^2)^{1/2}$ for an overall perspective, and the calculated ω_p decreases from 22 800 to 15 200 cm^{-1} across the phase transition. In the meantime, the scattering rates of the two components drop tremendously, from 720 to 32 cm^{-1} for the Drude 1 term and from 3310 to 854 cm^{-1} for the Drude 2 term as the temperature decreases from 300 to 5 K. The overall plasma frequency can also be estimated by partial summarization of the spectral weight $\omega_p = \sqrt{8 \int_0^{\omega_c} \sigma_1(\omega') d\omega'}$, where ω_c is the cutoff frequency for the Drude components. Taking the location of the conductivity minimum as the cutoff frequency,

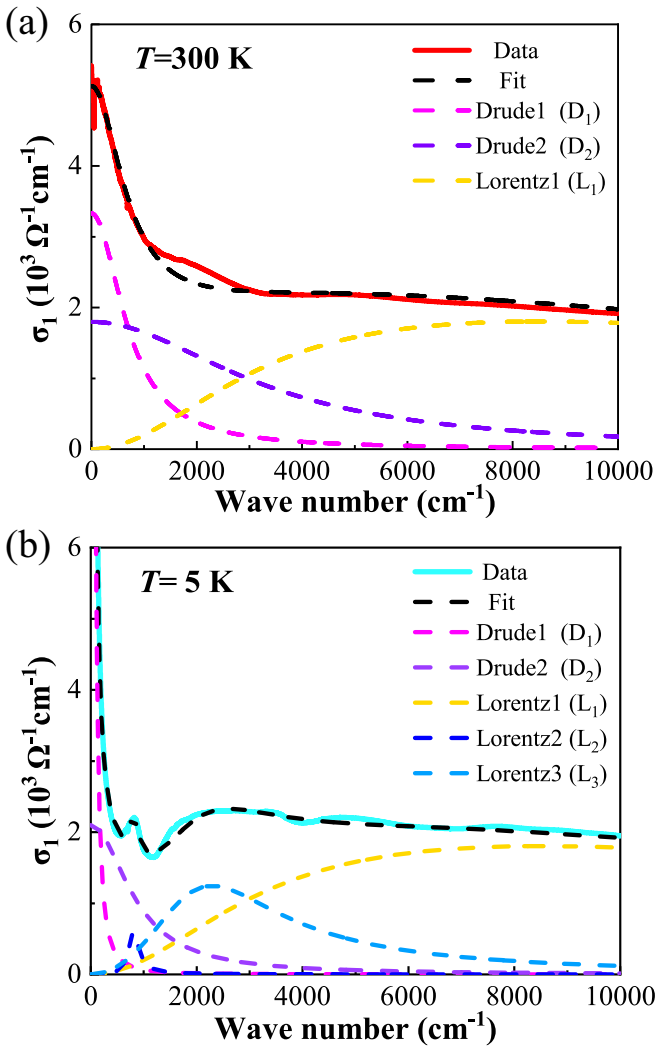

FIG. 3. Drude-Lorentz fitting of optical conductivity for $TaTe_2$. (a) $T = 300$ K. (b) $T = 5$ K.

near 3000 cm^{-1} for 300 K and 1000 cm^{-1} for 5 K, where the balance between the tails of Drude and Lorentz components is roughly taken into account, the obtained plasma frequency ω_p varies roughly from 1.9×10^4 cm^{-1} at 300 K to 1.4×10^4 cm^{-1} at 5 K. The obtained values of the plasma frequencies are close to the previous decomposition of the spectral weight. The change in the overall plasma frequency indicates a sudden reconstruction of the band structure. The sudden narrowing of the Drude components suggests the dramatic reduction of scattering rates of conduction carriers in the LT phase, which are also reflected in the fitting parameters in the above Lorentz-Drude model analysis. The sharp decrease of the scattering rate gives an even lower dc resistivity in the LT phase despite the significantly reduced spectral weights of the Drude components.

Our ultrafast pump-probe experiment provides further support that the structural phase transition is not of a conventional density wave type. The ultrafast pump-probe experiment with a standard reflection geometry configuration was performed in a Ti:sapphire amplified laser (Spitfire Ace) of 800-nm pulses for a duration of 35 fs at a 1 kHz repetition frequency. To minimize heating effect as much as possible, the fluence of the pump beam is set to around 90 $\mu J/cm^2$ while the probe beam is 30 times weaker than the pump beam. The spot size was determined to be 110 and 90 μm in diameter by a 100-μm-diameter pinhole for the pump and probe spots, respectively. The pump and probe pulses were set to be cross polarized and an extra grid polarizer was mounted just before the silicon detector (Thorlabs, DET36A2) in order to reduce the noise from stray light. Also, the probe pulses were split for balanced detection in order to improve the signal-to-noise ratio.

Figure 4(a) presents the photoinduced transient reflectivity as a function of time delay on a freshly cleaved $1T'$-$TaTe_2$ at a number of selected temperatures. All data were collected when the sample was warmed up from low temperature. A sudden change was found precisely at the phase transition temperature ($T_s \approx 160$ K). This sudden electron relaxation dynamics change was also observed just after the structural phase transition in $YbInCu_4$ and CsV_3Sb_5 [45,46]. Very prominently, with temperature increasing across T_s, the amplitude of the photoinduced $\Delta R/R$ is enhanced dramatically. The measurement reveals that the compound exhibits two quitely different electronic states just above and below the T_s.

In order to quantitatively analyze the relaxation of the photoexcited quasiparticles, we use a single-exponential function to fit the decay process, $\Delta R/R = A\exp(-t/\tau_d) + C$, where A in the formula represents the amplitude of the photoinduced reflectivity change, τ_d stands for the relaxation time, and C is constant for a long-lived thermal diffusion process. The best-fitting curves are shown as dashed lines in Fig. 4(a). The temperature dependence of the extracted fitting parameters A and τ_d of the single-exponential function are shown in Figs. 4(b) and 4(c). It is evident that the compound shows totally different behaviors above and below T_s. In the HT phase, the decay time of the relaxation process gradually increases from ~0.4 ps at 160 K to ~1.5 ps at 300 K, but becomes almost temperature independent in the LT phase with a much slower process seemingly at around 10 ps. The amplitude of the photoinduced reflectivity change varies little in the LT phase until the temperature rises close to T_s. With temperature changes across T_s, the amplitude suddenly increases from ~0.4 at 150 K to ~1.6 at 160 K and the whole increasing process is a typical steplike shape. Here, we have to emphasize that the parameters for the LT phase are at the limit of the error bar. For the HT phase, we can see a distinct decay process. However, the decay process becomes obscure in the LT phase due to the substantial reduction of amplitude of the reflectivity change as well as the appearance of many strong coherent phonon oscillations. In principle, one can subtract the coherent phonon oscillations, and extract the decay process to a more accurate level. In reality, it is rather challenging to fit so many phonon modes and uncertainties are inevitably introduced.

Ultrafast pump-probe spectroscopy also provides useful information about coherent phonon oscillations. After subtracting the electron dynamics background, we obtained the coherent phonon oscillations in Fig. 5(a). The fast Fourier transform (FFT) results are displayed in Fig. 5(b). A detailed two-dimensional intensity map as a function of temperature and frequency is presented in Fig. 5(c). The coherent phonon

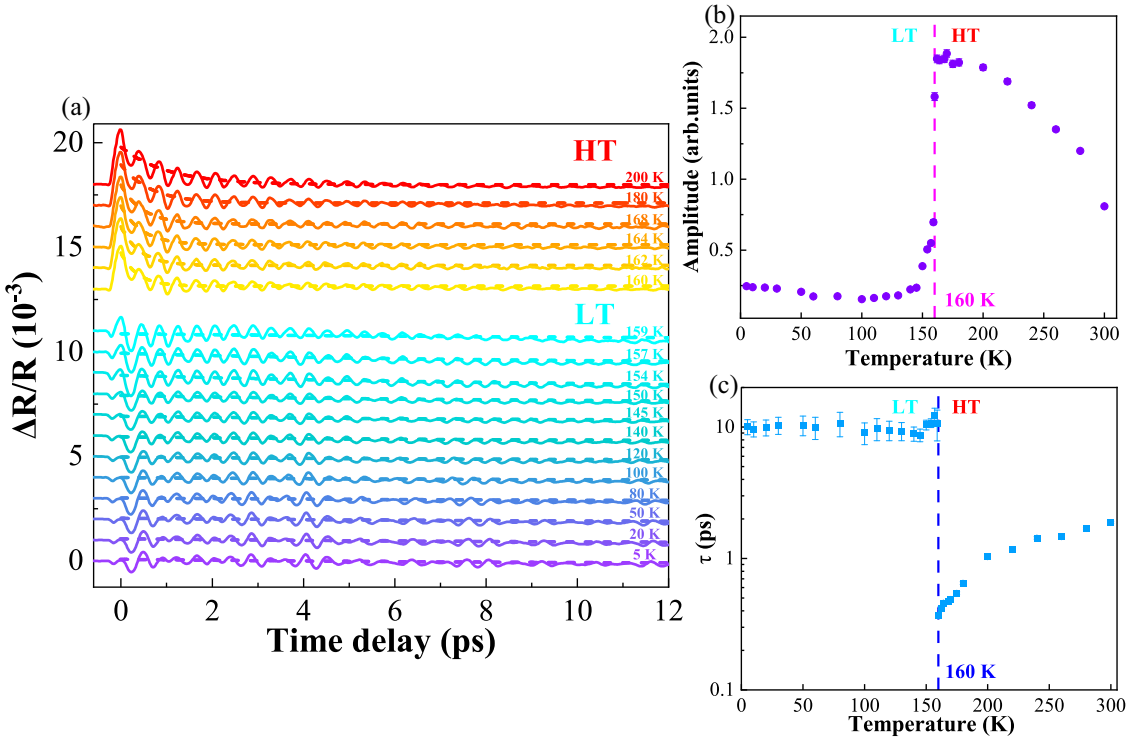

FIG. 4. Temperature-dependent ultrafast relaxation dynamics for $TaTe_2$. (a) $\Delta R/R$ in the temperature range of 5–200 K at some selected temperature points. The dashed lines are the single-exponential fitting curves: $\Delta R/R(t) = A\,e^{-t/\tau_d} + C$. The amplitude A (purple circles) in (b) and decay time in (c) (blue squares) of the transient reflectivity extracted from fits to the single exponential above and below the structural phase transition $T_s \approx 160$ K. Error bars represent the standard deviation of the fit.

frequencies are in agreement with the previous Raman experiment results on $TaTe_2$ [34]. In the HT phase, there are two distinct peaks at 2.4 and 3.3 THz in the frequency domain. In the LT phase, more phonon modes abruptly appear due to the symmetry lowering caused by Ta atoms clustering further, yielding evidence for a new structural modulation. Remarkably, a phonon at 3.3 THz even splits into one A_g mode phonon peak and one B_g mode phonon peak, which is in good agreement with the density functional theory (DFT) calculations for the LT phonon spectra [31]. The distinct phonon mode splitting near 3.3 THz further indicates that the phase transition is a first-order phase transition. On the other hand, a conventional CDW condensate also has collective excitations referred to as an amplitude mode and phase mode. Usually, the energy level of the amplitude mode is in the range of terahertz frequency which could be identified by an ultrafast pump-probe experiment [39–41,47–49]. The amplitude mode exhibits more pronounced oscillations with decreasing temperature and usually appears as the strongest oscillations. The mode frequency softens and behaves as an order parameter when the temperature gets close to the T_{CDW} [39]. Nevertheless, no such CDW amplitude mode could be identified from the above phonon spectra in the LT phase. Similarly, we noticed that an amplitude mode was also not observed in

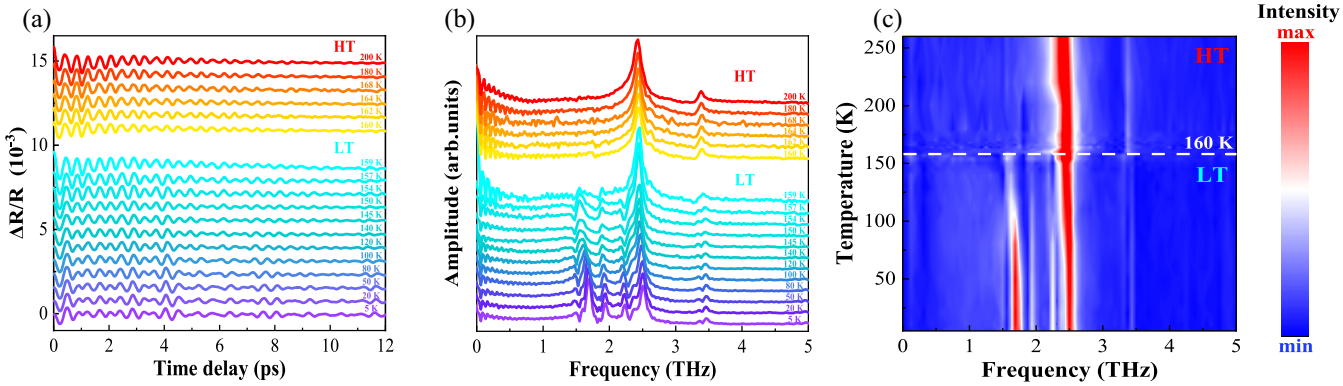

FIG. 5. Temperature-dependent coherent phonon spectroscopy for $TaTe_2$ in a time/frequency domain. (a) Coherent phonon oscillations result in a time domain after the decay background is subtracted. (b) The fast Fourier transformation (FFT) results of the data in (a). (c) Temperature-dependent intensity map extracted from (b).

the recently reported kagome metal CsV_3Sb_5 coherent phonon spectra in the LT CDW phase [46,50]. It could also suggest that the structural phase transition is not of a conventional density wave type.

The above pump-probe experiment results reveal a rather specific situation: There are two entirely different behaviors above and below the structural phase transition temperature. Both the transient reflectivity amplitude and decay time change dramatically. A number of coherent phonon modes suddenly appear in the LT phase without a clear trace of softening at the structural phase transition temperature. No observed phonon modes in the LT phase phonon spectra could be identified as the CDW amplitude mode. All those features are well consistent with the first-order phase transition and entirely different from the usual conventional second-order CDW condensate behaviors.

It is inspiring to compare the present results on $1T'$-$TaTe_2$ with the closest relative TaX_2 (X = S, Se). TaX_2 (X = S, Se) have both $2H$- and $1T$-type structures. They all show structural instabilities but exhibit different behaviors. For example, a gradual development of the CDW energy gap was observed below the structural transition temperature at 75 K for $2H$-TaS_2 [7]. A clear quasidivergence of the photoexcited carrier relaxation time in the decay dynamics and an order-parameter-like softening of the amplitude mode in approaching the transition temperature at 122 K were observed in the pump-probe measurement for $2H$-TaS_2 [48]. Those observations indicate that $2H$-type TaX_2 (X = S, Se) are similar to the conventional CDW compounds, such as rare-earth tritelluride RTe_3, $LaAgSb_2$, $Bi_2Rh_3Se_2$, and CuTe as we have mentioned above. However, for $1T$-$TaSe_2$, a number of phonon modes appear suddenly at the structural phase transition near 473 K in the pump-probe and Raman scattering experiments [51]. Although one of the modes with a stronger intensity at 2.0 THz was suggested to be a CDW amplitude mode, it actually shows little softening in approaching the structural phase transition [51]. A similar sudden change in the coherent phonon mode and relaxation dynamics was also observed for $1T$-TaS_2 [48]. Therefore, those $1T$-type TaX_2 (X = S, Se) are similar to the present study on $1T'$-$TaTe_2$ where the origins of the structural phase transitions are different from the $2H$-type compounds.

Based on our experiment results, we could infer that the origin of the structural phase transition at $T_s \approx 160$ K could not be attributed to a density-wave type instability, as many typical two-dimensional CDW systems, e.g., RTe_2 and RTe_3 (R = rare-earth metal) [38,52]. Apparently, further theoretical calculations and analyses are still needed to elucidate precisely the driving force of the structural phase transition in $1T'$-$TaTe_2$.

III. SUMMARY

In summary, we have performed a combined optical spectroscopy and ultrafast pump-probe study on single-crystal $1T'$-$TaTe_2$ in an effort to understand the electronic structure in the LT phase. The optical study revealed the electronic band structure reconstruction over a broad energy scale, and time-resolved pump-probe measurements provide further evidence that the first-order phase transition is irrelevant to conventional CDW order formation. Both studies indicated that the structural phase transition was not driven by conventional CDW instability. Our research on $1T'$-$TaTe_2$ would motivate further investigations on the origin or driving force of the phase transition.

ACKNOWLEDGMENTS

This work was supported by the National Key Research and Development Program of China (No. 2017YFA0302904), and the National Natural Science Foundation of China (No. 11888101).

[1] J. Wilson and A. Yoffe, Adv. Phys. **18**, 193 (1969).
[2] M. N. Ali, J. Xiong, S. Flynn, J. Tao, Q. D. Gibson, L. M. Schoop, T. Liang, N. Haldolaarachchige, M. Hirschberger, N. P. Ong, and R. J. Cava, Nature (London) **514**, 205 (2014).
[3] Y. Yu, F. Yang, X. F. Lu, Y. J. Yan, Y.-H. Cho, L. Ma, X. Niu, S. Kim, Y.-W. Son, D. Feng, S. Li, S.-W. Cheong, X. H. Chen, and Y. Zhang, Nat. Nanotechnol. **10**, 270 (2015).
[4] J. Wilson, F. D. Salvo, and S. Mahajan, Adv. Phys. **24**, 117 (1975).
[5] E. Morosan, H. W. Zandbergen, B. S. Dennis, J. W. G. Bos, Y. Onose, T. Klimczuk, A. P. Ramirez, N. P. Ong, and R. J. Cava, Nat. Phys. **2**, 544 (2006).
[6] T. Valla, A. V. Fedorov, P. D. Johnson, P.-A. Glans, C. McGuinness, K. E. Smith, E. Y. Andrei, and H. Berger, Phys. Rev. Lett. **92**, 086401 (2004).
[7] W. Z. Hu, G. Li, J. Yan, H. H. Wen, G. Wu, X. H. Chen, and N. L. Wang, Phys. Rev. B **76**, 045103 (2007).
[8] S. V. Borisenko, A. A. Kordyuk, V. B. Zabolotnyy, D. S. Inosov, D. Evtushinsky, B. Büchner, A. N. Yaresko, A. Varykhalov, R. Follath, W. Eberhardt, L. Patthey, and H. Berger, Phys. Rev. Lett. **102**, 166402 (2009).
[9] M. Van Maaren and G. Schaeffer, Phys. Lett. A **24**, 645 (1967).
[10] T. M. Rice and G. K. Scott, Phys. Rev. Lett. **35**, 120 (1975).
[11] A. H. Castro Neto, Phys. Rev. Lett. **86**, 4382 (2001).
[12] T. Kiss, T. Yokoya, A. Chainani, S. Shin, T. Hanaguri, M. Nohara, and H. Takagi, Nat. Phys. **3**, 720 (2007).
[13] M. D. Johannes and I. I. Mazin, Phys. Rev. B **77**, 165135 (2008).
[14] D. W. Shen, Y. Zhang, L. X. Yang, J. Wei, H. W. Ou, J. K. Dong, B. P. Xie, C. He, J. F. Zhao, B. Zhou, M. Arita, K. Shimada, H. Namatame, M. Taniguchi, J. Shi, and D. L. Feng, Phys. Rev. Lett. **101**, 226406 (2008).
[15] K. Rossnagel, J. Phys.: Condens. Matter **23**, 213001 (2011).
[16] J. van Landuyt, G. van Tendeloo, and S. Amelinckx, Phys. Status Solidi A **26**, 585 (1974).
[17] T. Sörgel, J. Nuss, U. Wedig, R. Kremer, and M. Jansen, Mater. Res. Bull. **41**, 987 (2006).
[18] Y. Liu, W. J. Lu, D. F. Shao, L. Zu, X. C. Kan, W. H. Song, and Y. P. Sun, Europhys. Lett. **109**, 17003 (2015).

[19] H. Chen, Z. Li, L. Guo, and X. Chen, Europhys. Lett. **117**, 27009 (2017).
[20] Y. Liu, D. F. Shao, L. J. Li, W. J. Lu, X. D. Zhu, P. Tong, R. C. Xiao, L. S. Ling, C. Y. Xi, L. Pi, H. F. Tian, H. X. Yang, J. Q. Li, W. H. Song, X. B. Zhu, and Y. P. Sun, Phys. Rev. B **94**, 045131 (2016).
[21] H. Luo, W. Xie, J. Tao, H. Inoue, A. Gyenis, J. W. Krizan, A. Yazdani, Y. Zhu, and R. J. Cava, Proc. Natl. Acad. Sci. USA **112**, E1174 (2015).
[22] J. Guo, H. Luo, H. Yang, L. Wei, H. Wang, W. Yi, Y. Zhou, Z. Wang, S. Cai, S. Zhang, X. Li, Y. Li, J. Liu, K. Yang, A. Li, J. Li, Q. Wu, R. J. Cava, and L. Sun, arXiv:1704.08106.
[23] B. E. Brown, Acta Crystallogr. **20**, 264 (1966).
[24] X. Zhang, T. Luo, X. Hu, J. Guo, G. Lin, Y. Li, Y. Liu, X. Li, J. Ge, Y. Xing, Z. Zhu, P. Gao, L. Sun, and J. Wang, Chin. Phys. Lett. **36**, 057402 (2019).
[25] J. J. Yang, Y. J. Choi, Y. S. Oh, A. Hogan, Y. Horibe, K. Kim, B. I. Min, and S.-W. Cheong, Phys. Rev. Lett. **108**, 116402 (2012).
[26] A. F. Fang, G. Xu, T. Dong, P. Zheng, and N. L. Wang, Sci. Rep. **3**, 1153 (2013).
[27] D. Ootsuki, S. Pyon, K. Kudo, M. Nohara, M. Horio, T. Yoshida, A. Fujimori, M. Arita, H. Anzai, H. Namatame, M. Taniguchi, N. L. Saini, and T. Mizokawa, J. Phys. Soc. Jpn. **82**, 093704 (2013).
[28] S. Sharma, L. Nordström, and B. Johansson, Phys. Rev. B **66**, 195101 (2002).
[29] D. C. Miller, S. D. Mahanti, and P. M. Duxbury, Phys. Rev. B **97**, 045133 (2018).
[30] C. Chen, H.-S. Kim, A. S. Admasu, S.-W. Cheong, K. Haule, D. Vanderbilt, and W. Wu, Phys. Rev. B **98**, 195423 (2018).
[31] J. J. Gao, J. G. Si, X. Luo, J. Yan, F. C. Chen, G. T. Lin, L. Hu, R. R. Zhang, P. Tong, W. H. Song, X. B. Zhu, W. J. Lu, and Y. P. Sun, Phys. Rev. B **98**, 224104 (2018).
[32] V. Petkov, K. Chapagain, J. Yang, S. Shastri, and Y. Ren, Phys. Rev. B **102**, 024111 (2020).
[33] I. El Baggari, N. Sivadas, G. M. Stiehl, J. Waelder, D. C. Ralph, C. J. Fennie, and L. F. Kourkoutis, Phys. Rev. Lett. **125**, 165302 (2020).
[34] Y.-C. Luo, Y.-Y. Lv, R.-M. Zhang, L. Xu, Z.-A. Zhu, S.-H. Yao, J. Zhou, X.-X. Xi, Y. B. Chen, and Y.-F. Chen, Phys. Rev. B **103**, 064103 (2021).
[35] K. M. Siddiqui, D. B. Durham, F. Cropp, C. Ophus, S. Rajpurohit, Y. Zhu, J. D. Carlström, C. Stavrakas, Z. Mao, A. Raja, P. Musumeci, L. Z. Tan, A. M. Minor, D. Filippetto, and R. A. Kaindl, Commun. Phys. **4**, 152 (2021).
[36] I. Kar, K. Dolui, L. Harnagea, Y. Kushnirenko, G. Shipunov, N. C. Plumb, M. Shi, B. Büchner, and S. Thirupathaiah, J. Phys. Chem. C **125**, 1150 (2021).
[37] D. B. Tanner, Phys. Rev. B **91**, 035123 (2015).
[38] B. F. Hu, B. Cheng, R. H. Yuan, T. Dong, and N. L. Wang, Phys. Rev. B **90**, 085105 (2014).
[39] R. Y. Chen, S. J. Zhang, M. Y. Zhang, T. Dong, and N. L. Wang, Phys. Rev. Lett. **118**, 107402 (2017).
[40] T. Lin, L. Y. Shi, Z. X. Wang, S. J. Zhang, Q. M. Liu, T. C. Hu, T. Dong, D. Wu, and N. L. Wang, Phys. Rev. B **101**, 205112 (2020).
[41] R. S. Li, L. Yue, Q. Wu, S. X. Xu, Q. M. Liu, Z. X. Wang, T. C. Hu, X. Y. Zhuo, L. Y. Shi, S. J. Zhang, D. Wu, T. Dong, and N. L. Wang, arXiv:2110.01502.
[42] Z. G. Chen, G. Xu, W. Z. Hu, X. D. Zhang, P. Zheng, G. F. Chen, J. L. Luo, Z. Fang, and N. L. Wang, Phys. Rev. B **80**, 094506 (2009).
[43] R. Y. Chen, Y. G. Shi, P. Zheng, L. Wang, T. Dong, and N. L. Wang, Phys. Rev. B **91**, 125101 (2015).
[44] S.-i. Kimura, Y. Nakajima, Z. Mita, R. Jha, R. Higashinaka, T. D. Matsuda, and Y. Aoki, Phys. Rev. B **99**, 195203 (2019).
[45] M. Y. Zhang, R. Y. Chen, T. Dong, and N. L. Wang, Phys. Rev. B **95**, 165104 (2017).
[46] Z. X. Wang, Q. Wu, Q. W. Yin, C. S. Gong, Z. J. Tu, T. Lin, Q. M. Liu, L. Y. Shi, S. J. Zhang, D. Wu, H. C. Lei, T. Dong, and N. L. Wang, Phys. Rev. B **104**, 165110 (2021).
[47] J. Demsar, K. Biljaković, and D. Mihailovic, Phys. Rev. Lett. **83**, 800 (1999).
[48] J. Demsar, L. Forró, H. Berger, and D. Mihailovic, Phys. Rev. B **66**, 041101(R) (2002).
[49] R. V. Yusupov, T. Mertelj, J.-H. Chu, I. R. Fisher, and D. Mihailovic, Phys. Rev. Lett. **101**, 246402 (2008).
[50] N. Ratcliff, L. Hallett, B. R. Ortiz, S. D. Wilson, and J. W. Harter, Phys. Rev. Materials **5**, L111801 (2021).
[51] C. J. Sayers, H. Hedayat, A. Ceraso, F. Museur, M. Cattelan, L. S. Hart, L. S. Farrar, S. Dal Conte, G. Cerullo, C. Dallera, E. Da Como, and E. Carpene, Phys. Rev. B **102**, 161105(R) (2020).
[52] D. R. Garcia, G.-H. Gweon, S. Y. Zhou, J. Graf, C. M. Jozwiak, M. H. Jung, Y. S. Kwon, and A. Lanzara, Phys. Rev. Lett. **98**, 166403 (2007).